Frontiers in Bioscience Landmark

Front. Biosci. (Landmark Ed) **2026**; 31(10): 54858
https://doi.org/10.31083/FBL54858

Original Research

Ganoderma lucidum Polysaccharides Alleviate Diabetic Cardiomyopathy Structural Deficits and Remodeling by Attenuating Inflammatory Responses

Changlin Zhen[1,2,*], Guoli Li[1,2], Feng Chen[3], Dan Liu[1,2], Xiuzhen He[1,2], Jiawei Miao[1,2], Yifan Yan[4]

[1]School of Basic Medical Sciences, Chongqing Three Gorges Medical College, 404120 Chongqing, China
[2]Natural Drug Intervention in Aging Key Laboratory of Chongqing Education Commission of China, Chongqing Key Laboratory of Development and Utilization of Genuine Medicinal Materials in Three Gorges Reservoir Area, 404120 Chongqing, China
[3]Chongqing Tangshikang Medical Technology Co., Ltd., 404120 Chongqing, China
[4]School of Medical Technology, Chongqing Three Gorges Medical College, 404120 Chongqing, China
*Correspondence: changlinzhen@cqtgmc.edu.cn (Changlin Zhen)
Academic Editor: Graham Pawelec
Submitted: 13 June 2026 Revised: 22 July 2026 Accepted: 3 August 2026 Published: 15 October 2026

Abstract

Background: Diabetes is the one of the most prevalent chronic diseases worldwide and poses a serious danger to human health, following cancer and cardiovascular and cerebrovascular diseases. Diabetic cardiomyopathy (DCM) is a leading cause of death among individuals with diabetes. *Ganoderma lucidum* polysaccharides (GLPs) are among the principal bioactive components in the fruiting bodies of *Ganoderma lucidum*, and are characterized by complex structures and a range of pharmacological properties. In several studies, GLPs have been shown to exert hypoglycemic effects and to help normalize dysregulated glucose metabolism. Our team has also previously demonstrated the ability of GLPs to inhibit cardiac hypertrophy induced by increased cardiac afterload. However, systematic investigations ofthe effects of GLPs in DCM remain limited, and the molecular mechanisms through which GLPs shape DCM pathogenesis remain unclear. **Methods:** We investigated the effects of *Ganoderma lucidum* polysaccharides (GLPs) on diabetic cardiomyopathy (DCM) in mouse models of streptozotocin-induced type 1 diabetes mellitus (T1DM) and high-fat diet-induced type 2 diabetes mellitus (T2DM). **Results:** We found that GLPs exerted therapeutic effects in murine models of both T1DM and T2DM. RNA-seq analysis suggested that the anti-inflammatory of GLPs involve nuclear factor-kappa B (NF-κB) signaling. Cardiac inflammation is a key pathological process in DCM, and GLP treatment attenuated cardiac functional and structural abnormalities while reducing cardiac inflammation, fibrosis, and NF-κB signaling. GLP administration further reduced DCM-associated increases in pro-inflammatory cytokines and macrophage infiltration in T1DM and T2DM mice. *In vitro*, GLPs suppressed high glucose (HG)-induced cardiac hypertrophy and fibrosis, and the protective effects of GLPs were associated with NF-κB signaling. **Conclusions:** Collectively, our findings demonstrate that GLPs effectively alleviate DCM and cardiac remodeling and the protective effects of GLPs are involved in NF-κB signaling. Our data suggest that GLPs may serve as a potential therapeutic agent for the treatment of DCM.

Keywords: diabetic cardiomyopathy; *Ganoderma lucidum* polysaccharides; inflammation; nuclear factor kappa-B

1. Introduction

Diabetes is the third most common chronic disease worldwide following cancer and cardiovascular and cerebrovascular diseases, and poses a serious threat to global public health. Diabetic cardiomyopathy (DCM) is one of the leading causes of death in people with diabetes, making it a complication of particular concern [1,2,3,4,5]. The pathogenesis of DCM is multifaceted, encompassing mitochondrial impairment, oxidative injury, inflammatory responses, programmed cell death, autophagic dysregulation, myocardial fibrotic remodeling, and lipotoxic insults [6]. Sustained inflammation is regarded as a critical contributor to DCM pathogenesis [7]. Persistent inflammation and elevated levels of inflammatory mediators contribute to the pathological alterations observed in the diabetic myocardium [8]. Elevated levels of inflammatory cytokines such as tumor necrosis factor-α (TNF-α), interleukin-6 (IL-6), and interleukin-1 (IL-1β) have been linked to hyperglycemic conditions and contribute to the initiation or aggravation of myocardial damage, thereby promoting maladaptive cardiac remodeling. In this context, the transcription factor nuclear factor-kappa B (NF-κB) plays a central role in regulating pro-inflammatory gene transcription. Activation of the NF-κB signaling cascade represents a convergent inflammatory process that has been widely implicated in diabetic myocardial inflammation [9,10,11,12]. The limited availability of effective preventive and therapeutic options for DCM stems largely from its complex pathophysiology, underscoring the pressing need for the development of novel pharmacological strategies.

Ganoderma lucidum is a prized traditional Chinese medicine characterized by a range of pharmacological ef-

Copyright: © 2026 The Author(s). Published by IMR Press.
This is an open access article under the CC BY 4.0 license.

Publisher's Note: IMR Press stays neutral with regard to jurisdictional claims in published maps and institutional affiliations.

fects. The medicinal properties of *Ganoderma lucidum* cover a broad spectrum of indications, ranging from oncological, allergic, cardiovascular, pulmonary, neurologic, metabolic, hepatic, rheumatic, and hematologic disorders to immunomodulation, senescence retardation, and oxidative stress alleviation [13]. To date, over 400 secondary metabolites have been isolated from *Ganoderma lucidum*, including bioactive components such as *Ganoderma lucidum* polysaccharides (GLPs), triterpenoids, proteins, and peptides, all of which offer a high degree of medicinal value. As the most abundant and functionally important bioactive molecules in the sporocarps of *G. lucidum*, GLPs are characterized by intricate molecular structures and a broad spectrum of clinically relevant bioactivities.

Many studies have reported on the hypoglycemic effects of GLPs and their ability to remediate dysregulated glucose metabolism [14]. Studies have shown that the GLP treatment of streptozotocin-induced diabetic rats led to a dose-dependent reduction in blood glucose concentrations, with *in vitro* islet cell experiments having additionally revealed that the hypoglycemic effects of GLPs may be related to their ability to shield islet cells from free radical-induced damage [15]. In addition to reducing Bax expression at the mRNA level, GLPs have also been found to upregulate the mRNA levels of genes encoding B-cell lymphoma-2 (Bcl-2) and Pancreatic and duodenal homeobox 1 (PDX-1), thereby inhibiting islet cell apoptosis and improving insulin resistance [16]. GLPs thus exhibit good preventive and therapeutic effects in diabetes. Other studies have further shown that GLPs can protect the cardiovascular system by preventing cardiomyocyte damage [17]. GLPs protect the myocardium by reducing malondialdehyde levels, activating antioxidant enzymes glutathione peroxidase (GSH-Px), catalase (CAT) and superoxide dismutase (SOD) in myocardial tissue, and alleviating lipid peroxidation in rat models of type 2 diabetes mellitus (T2DM). In addition, GLPs can alter cardiac function and significantly improve myocardial ultrastructure in T2DM model rats [18]. In patients with atrial fibrillation, GLPs have been shown to exert cardioprotective effects that manifest as significant reductions in systolic and diastolic blood pressure, heart rate, and inflammatory factors such as IL-1β, IL-6, hsCRP, and TNF-α [19]. In a previous study, we also found that GLPs can abrogate cardiac hypertrophy induced by increased cardiac afterload [20]. Moreover, multiple studies have shown that GLPs exert anti-inflammatory effects by inhibiting the NF-κB signaling pathway [21,22,23,24]. However, systematic studies exploring the function of GLPs in DCM are currently lacking, and the molecular mechanisms by which GLPs regulate DCM pathogenesis remain unclear. An in-depth exploration of the mechanistic effects of GLPs as regulators of DCM is thus urgently needed to inform the clinical diagnosis and treatment of this condition.

In the present study, we found that GLP treatment can prevent cardiac inflammation and fibrosis in diabetic model mice and inhibit the inflammatory and fibrotic changes in cardiomyocytes induced by exposure to high glucose (HG) conditions. Notably, GLPs were found to be capable of mitigating the HG-induced inflammatory activation of myocardial cells. The NF-κB signaling cascade was further identified as a key effector pathway through which GLPs exert their anti-inflammatory activity. Together, our results suggest that GLPs represent a novel potential therapeutic candidate for the treatment of DCM.

2. Materials and Methods

2.1 Animal Experiments

C57BL/6 mice were purchased from Cyagen Biosciences (Guangzhou, China). Mice were maintained in an SPF environment (20–26 °C, 40–70% humidity, 12/12 h light–dark cycle) with unrestricted food and water, and were randomly assigned to different experimental groups. GLP powder (≥95% purity by UV assay) was commercially acquired from ESITEBiogle (Chengdu, China) and reconstituted in sterile normal saline. Based on the exploratory nature of the study and previous similar reports, no formal sample size calculation was performed, and 6 mice per group were used [25]. All mice were randomly assigned to different groups using a random number table method after acclimatization to housing conditions. To ensure allocation concealment, both the animal caretakers and the experiment operators were blinded to group assignments prior to experiment initiation, and the blinding was maintained until experimental procedures and data analyses were complete. This study employed a double-blind design such that investigators responsible for the experimental procedures were unaware of group allocations. Drugs were prepared by a third-party individual and labeled with coded identifiers to ensure that the administering operators could not distinguish between treatments. During the outcome assessment phase, all evaluations were independently performed by two investigators who were blinded to group assignments in order to minimize detection bias.

To establish a streptozotocin (STZ)-induced model of type 1 diabetes mellitus (T1DM) [25], 6-week-old male C57BL/6 mice (n = 6 per group) received daily intraperitoneal injections of STZ (50 mg/kg) dissolved in 0.1 mol/L sodium citrate buffer (pH 4.5) for five consecutive days. Age-matched control mice (n = 6) were injected with citrate buffer. On day 7, blood glucose levels were measured using a glucometer, and those mice with a fasting blood glucose exceeding 16.6 mM were considered diabetic. At 7 weeks post diabetes onset, 12 diabetic mice were randomly assigned to two equal-sized groups: untreated GLPs mice (T1DM) and GLPs-treated (25, 50, 100, 150 $mg \cdot kg^{-1} \cdot day^{-1}$) mice (GLPs+T1DM). GLPs were administered via oral gavage once per day from weeks 8 to 16. The T1DM and age-matched control groups received

normal saline alone on the same schedule. All animals had free access to water. Control mice (CON) and GLP-administered mice (GLPs) were fed a low-fat diet (LFD). Mice in the T1DM and GLPs+T1DM groups were fed a high-fat diet (HFD). The LFD provided 10 kcal% fat, 20 kcal% protein, and 70 kcal% carbohydrate (MediScience Diets, Yangzhou, China; #MD12031), whereas the HFD provided 60 kcal% fat, 20 kcal% protein, and 20 kcal% carbohydrate (#MD12033). Normal saline was used as a vehicle for GLP administration.

To establish a T2DM model [26], 24 male C57BL/6 mice were randomized into four groups (n = 6 per group): LFD (CON), HFD (T2DM), LFD supplemented with GLPs (GLPs), and HFD with GLPs (25, 50, 100, 150 $mg \cdot kg^{-1} \cdot day^{-1}$; T2DM+GLPs). All mice were maintained on their respective diets for 24 weeks. From week 16 to week 24, GLPs were administered via oral gavage once per day to the HFD+GLPs group. The HFD and LFD control groups received equal volumes of the vehicle on the same schedule.

During the experimental period, all animals survived, with body weight and blood glucose being monitored on a weekly basis. After treatment was complete, the mice were sacrificed under anesthesia, and both blood and cardiac specimens were obtained. Serum biomarkers of myocardial damage, including lactate dehydrogenase (LDH) and cardiac creatine kinase (CK-MB), were evaluated, while cardiac atrial natriuretic peptide (ANP) and B-type natriuretic peptide (BNP) mRNA levels were assessed by reverse transcription-quantitative real-time polymerase chain reaction (RT-qPCR). Excised cardiac tissues were then processed either by snap-freezing in liquid nitrogen for later molecular profiling or by immersion in 4% paraformaldehyde for histopathological analysis.

2.2 Euthanasia Procedure

For tissue collection at study termination, all mice were humanely euthanized. Anesthesia was induced by placing each animal in a chamber with 3% isoflurane in 100% O_2 (1–2 L/min), and the loss of pedal and corneal reflexes was used to confirm surgical-level anesthesia. Decapitation was then performed for euthanasia; in cases where rapid tissue harvesting was essential, decapitation followed immediately after induction to forestall any return of consciousness. These manipulations were undertaken by experienced staff in accordance with applicable institutional and national animal welfare regulations. Following euthanasia, specimens of interest were promptly harvested.

2.3 Cell Culture Studies

Neonatal Sprague-Dawley (SD) rats were purchased from Chongqing Medical University Animal Experiment Center (Chongqing, China). Neonatal rat ventricular myocytes (NRVMs) were isolated from rats within three days of birth. Anesthesia was induced by placing each animal in a chamber with 3% isoflurane in 100% O_2 (1–2 L/min), and the loss of pedal and corneal reflexes was used to confirm surgical-level anesthesia. Decapitation was then performed for euthanasia. Following euthanasia of the neonatal pups, hearts were rapidly harvested and flushed with PBS to clear blood contamination. Tissues were digested using a cocktail containing pancreatin (0.8 mg/mL, T8150, Solarbio, Beijing) and collagenase (0.625 mg/mL, BY06021, Boyun Biotech, Shanghai). Subsequent differential plating allowed for the enrichment of primary cardiomyocytes by removing adherent fibroblasts. Purified cells were then cultured in DMEM (4.5 g/L glucose) supplemented with 10% fetal bovine serum and 5-BrdU (0.1 mM, HY-15910, MedChemExpress, NJ, USA) in a humidified 5% CO_2 incubator at 37 °C. After 48 hours, evidence of regular spontaneous beating was considered indicative of cardiomyocytes that were suitable for use in subsequent experiments. All cells were validated by STR profiling and tested negative for mycoplasma.

2.4 Echocardiography

Cardiac function was assessed in anesthetized mice via transthoracic echocardiography using a Vevo 3100 system (Visual Sonics, Toronto, ON, Canada). Left ventricular function was assessed as per the manufacturer's guidelines based on key indices including LVIDd (end-diastolic dimension), LVIDs (end-systolic dimension), ejection fraction (EF%), and fractional shortening (FS%).

2.5 Histology

After PBS perfusion, hearts were fixed in 4% paraformaldehyde. For morphometric analysis, hematoxylin and eosin (H&E)-stained sections were used to quantify cardiomyocyte cross-sectional area as reported previously [27]. Parallel sections underwent Masson's trichrome staining to assess collagen deposition.

2.6 Immunofluorescence Microscopy

Immunofluorescence staining was performed in accordance with established protocols [28]. Drug-treated cardiomyocytes were sequentially fixed in 4% formaldehyde, permeabilized in 0.2% Triton X-100, and immunolabeled with primary antibodies targeting either α-actinin (Proteintech, 11313-2-AP, 1:500) or p65 (CST, 8242, 1:100), followed by visualization with a fluorescently labeled donkey anti-rabbit secondary IgG (Jackson ImmunoResearch, 711-545-152, 1:200). Cells were observed under a fluorescence microscope (Leica Wetzlar, Hesse, Germany), and cardiomyocyte area was measured using Image-Pro Plus 6.0 (Rockville, MD, USA). Scale calibration was performed based on the image to convert pixel units to micrometers, and the circular tool was used to delineate and measure cellular area.

Paraffin-embedded tissue sections were incubated overnight at 4 °C with antibodies against CD45 (ab10558,

Table 1. RT-qPCR primer sequences.

Gene Name	Forward primer	Reverse primer
Tgfb1 (mouse)	F:5′-CTCCCGTGGCTTCTAGTGC-3′	R:5′-GCCTTAGTTTGGACAGGATCTG-3′
Col1a1 (mouse)	F:5′-AATGGTGCTCCTGGTATTGC-3′	R:5′-GGTCCTCGTTTTCCTTCTT-3′
Myh7 (mouse)	F:5′-CAAAGGCAAGGCAAAGAAAG-3′	R:5′-TCACCCCTGGAGACTTTGTC-3′
Tnf-α (mouse)	F:5′-CAGGGGCCACCACGCTCTTC-3′	R:5′-TTTGTGAGTGTGAGGGTCTGG-3′
Anp (mouse)	F:5′-TCCGATAGATCTGCCCTCTT-3′	R:5′-CTCCAATCCTGTCAATCCTACC-3′
Bnp (mouse)	F:5′-ACCACCTTTGAAGTGATCCTATT-3′	R:5′-GCAAGTTTGTGCTCCAAGATAAG-3′
IL-6 (mouse)	F:5′-TAGTCCTTCCTACCCCAATTTCC-3′	R:5′-TTGGTCCTTAGCCACTCCTTC-3′
IL-1β (mouse)	F:5′-ACTCCTTAGTCCTCGGCCA-3′	R:5′-CCATCAGAGGCAAGGAGGAA-3′
Gapdh (mouse)	F:5′-GTGGCAAAGTGGAGATTGTTG-3′	R:5′-CGTTGAATTTGCCGTGAGTG-3′
Gapdh (rat)	F:5′-CATCTCCCTCACAATTCCATCC-3′	R:5′-GAGGGTGCAGCGAACTTTAT-3′
Cola1 (rat)	F:5′-GACATCCCTGAAGTCAGCTGC-3′	R:5′-TCCCTTGGGTCCCTCGAC-3′
Myh7 (rat)	F:5′-GAGGAGAGGGCGGACATT-3′	R:5′-ACTCTTCATTCAGGCCCTTG-3′
Tgfb1 (rat)	F:5′-GCAACAACGCAATCTATGAC-3′	R:5′-CCTGTATTCCGTCTCCTT-3′

Abcam) and CD68 (ab125212, Abcam), followed by a 30-minute incubation with a horseradish peroxidase (HRP) reagent at 37 °C. Following DAB incubation, sections were photographed using a fluorescence microscope (Leica, Wetzlar, Germany), with subsequent densitometric analysis being performed in Image-Pro Plus 6.0.

2.7 Western Blotting

Following the lysis of cultured cells and cardiac tissues, protein quantification was performed via BCA assay (Beyotime). For Western blotting, equal amounts of protein (10 μg per lane) were resolved via SDS-PAGE and subsequently electrotransferred onto PVDF membranes. After membranes had been blocked with 5% BSA, they were probed with appropriate primary antibodies at 4 °C overnight, followed by incubation with HRP-linked secondary antibodies (ZSGB-BIO) for 1 h. Chemiluminescent detection was carried out on a Bio-Rad ChemiDoc MP system with densitometric quantification of band intensity. Utilized primary antibodies were as follows: anti-Myh7 (Proteintech, 22280-1-AP, 1:2000), anti-COL1 (Proteintech, 66761-1-Ig, 1:2000), anti-TGF-β1 (Proteintech, 81746-2-RR, 1:2000), anti-p65 (Proteintech, 80979-1-RR, 1:1000), anti-phospho-p65 (Proteintech, 82335-1-RR, 1:1000), anti-IκBα (ABclonal, A19714, 1:2000), anti-phospho-IκBα (ABclonal, AP0999, 1:1000), and anti-β-tubulin (Abcam, ab6046, 1:1000).

2.8 Quantitative Real-Time PCR

Total RNA was isolated from murine cardiac tissues and cultured cardiomyocytes using the TRIzol reagent (Beyotime, Shanghai) in accordance with the manufacturer's instructions. First-strand cDNA synthesis was then performed using 1 μg of RNA template and a reverse transcription kit (Yeasen Biotech). All RT-qPCR reactions were run on an ABI 9500 platform (Applied Biosystems) with SYBR Green qPCR Master Mix (Yeasen). *Gapdh* was selected as the endogenous control, and gene expression levels were normalized using the $2^{-\Delta\Delta Ct}$ method. All primer pairs are detailed in Table 1.

2.9 RNA-Seq Library Preparation and Sequencing

Total RNA was isolated using the TRIzol reagent (Beyotime, Shanghai). RNA-seq libraries were prepared using a custom protocol based on Smart-seq2 [29,30]. The pre-amplified cDNA was fragmented using the Tn5 enzyme, and libraries were then generated using a TruePrep DNA Library Prep Kit V2 for Illumina (Vazyme Biotech, Nanjing, Jiangsu, China). Libraries were then subjected to paired-end sequencing on the Illumina HiSeq X Ten platform. SMRTbell™ template preparation was performed according to the manufacturer's guidelines. Raw sequencing reads from the PacBio RSII SMRT cells were processed using the SMRT-Portal analysis suite (Pacific Biosciences, Menlo Park, CA, USA) to obtain subread sequences for further analysis. Illumina HiSeq X Ten employs the "sequencing-by-synthesis" technology, which produces relatively short reads (e.g., paired-end 150 bp) but with high accuracy. It enables precise comparison of gene expression levels and is used to construct conventional RNA-seq libraries for studying the expression dynamics and regulatory networks of the overall transcriptome. PacBio RS II / SMRTbell RNA-seq is based on the single-molecule real-time (SMRT) sequencing technology platform. Its core advantage lies in its ultra-long read lengths, which allow direct sequencing of full-length cDNA molecules. This capability enables the discovery of many novel gene loci and transcript isoforms that are not annotated in the reference genome, thereby improving genome annotation.

2.10 Statistical Analyses

Data were analyzed using GraphPad Prism 9.5.1. All data are reported as mean ± standard error of the mean (SEM). For longitudinal comparisons, repeated-measures ANOVAs were employed, while comparisons among multiple groups were made with one-way ANOVAs and Bon-

ferroni's post hoc test. Between-group differences were assessed using Student's unpaired *t*-tests. The significance threshold was $p < 0.05$.

3. Results

3.1 GLP Treatment Alleviates Cardiac Functional and Structural Impairment in STZ-Induced T1DM Mice

To evaluate the therapeutic efficacy of GLPs, we first subjected 7-week-old male C57BL/6 mice to STZ-induced DCM modeling, followed by oral administration of GLPs (25, 50, 100, 150 mg/kg) from 8–16 weeks. Treatment with GLPs (100, 150 mg/kg) led to a significant decrease in fasting blood glucose levels in these T1DM mice (Fig. 1A), with no significant difference in the magnitude of this hypoglycemic effect between these two dose levels. Therefore, we selected 100 mg/kg as the *in vivo* administration dose for subsequent analyses. Survival analyses revealed no evidence of toxicity associated with this 100 mg/kg GLP dose level over the study duration (Fig. 1B). Echocardiographic analysis of T1DM mice demonstrated both systolic dysfunction and cardiac hypertrophy, manifested as a marked decline in EF% and FS% together with increased LVIDs and LVIDd, indicative of left ventricular chamber dilation (Fig. 1C–G). Treatment with GLPs significantly attenuated these structural abnormalities, as indicated by the diminished LVIDd and LVIDs (Fig. 1C–E). In agreement with the above results, treatment with GLPs produced marked anti-hypertrophic effects, as reflected by a decreased HW/TL ratio (Fig. 1F). The cardioprotective effects of GLPs were further confirmed by the restoration of EF% and FS% to normal levels in these STZ-induced diabetic mice, consistent with the reversal of cardiac dysfunction (Fig. 1G). ANP and BNP are established biomarkers of heart failure [31,32]. While T1DM model mice exhibited elevated mRNA levels for both *Anp* and *Bnp*, this upregulation was abolished by GLP administration (Fig. 1H,I). We next assessed serum LDH and CK-MB as indicators of cardiac injury to determine whether GLPs exert cardioprotective effects. In these animals, GLPs treatment significantly decreased levels of both of these markers (Fig. 1J,K). Together, these data suggest that GLPs protect against the development of cardiac damage in T1DM mice. H&E staining was additionally performed to evaluate cardiac morphology, which revealed that T1DM mouse hearts exhibited structural remodeling and hypertrophy—changes that were not observed following GLPs treatment (Fig. 1L,M). These results indicate that GLPs protect T1DM mice from both functional and structural cardiac deficits.

3.2 GLPs Attenuate STZ-Induced Cardiac Fibrosis

In light of the pivotal roles that fibrosis and inflammation play in STZ-induced cardiac failure, we next investigated the anti-fibrotic potential of GLPs in T1DM model mice. Masson's trichrome staining demonstrated that GLPs inhibited the development of cardiac fibrosis in these animals (Fig. 2A,B). Further evidence for the protective action of GLPs in T1DM came from the observed suppression of the fibrotic markers myosin heavy chain (MYHC), collagen type I (COL1), and transforming growth factor-β (TGF-β) at both the protein and mRNA levels (Fig. 2C–I). Collectively, these findings demonstrate that GLPs attenuate STZ-induced cardiac fibrosis in mice.

3.3 GLPs Mitigate HFD-Induced Cardiac Dysfunction and Structural Pathology in T2DM Mice

To corroborate the cardioprotective effects of GLPs in the context of T2DM, we conducted analogous experiments using HFD-fed mice. Following a 24-week HFD feeding regimen, cardiac function was evaluated in male C57BL/6 mice. In T2DM mice, treatment with GLPs (25, 50, 100, 150 mg/kg) markedly reduced fasting blood glucose levels, mirroring the hypoglycemic effect previously noted in STZ-induced T1DM models (Fig. 3A). As above, no difference in the magnitude of the hypoglycemic effect was evident when comparing the 100 mg/kg and 150 mg/kg, we selected 100 mg/kg as the *in vivo* administration dose for subsequent analyses. Survival curves revealed no evidence of toxicity for this GLP dose in treated mice (Fig. 3B). Echocardiographic evaluation revealed clear signs of cardiac dysfunction and dilation in T2DM mice, as evidenced by reduced EF% and FS% together with elevated LVIDd and LVIDs, indicative of hypertrophic remodeling (Fig. 3C–G). Administration of GLPs effectively reversed these abnormalities, yielding a marked reduction in both LVIDs and LVIDd (Fig. 3C–E), accompanied by a decrease in HW/TL (Fig. 3F). The cardioprotective effect of GLPs was further confirmed in T2DM mice, where treatment restored EF% and FS% to normal levels, thereby reversing the observed cardiac dysfunction (Fig. 3G). While T2DM mice exhibited elevated mRNA levels of *Anp* and *Bnp*, this effect was abolished in those receiving GLPs (Fig. 3H,I). We next examined serum LDH and CK-MB levels as a measure of cardiac injury in T2DM mice and found that GLPs treatment markedly reduced the levels of both of these markers (Fig. 3J,K). Together, these data suggest that GLPs prevent heart damage in T2DM mice. H&E staining was performed to evaluate cardiac morphology, revealing that the hearts of T2DM model animals exhibited pronounced hypertrophy and structural disorganization, while these changes were effectively prevented by GLPs treatment (Fig. 3L,M). These data collectively demonstrate that GLPs attenuate both cardiac dysfunction and structural damage in HFD-fed T2DM mice.

3.4 GLPs Ameliorate Myocardial Fibrosis in HFD-Fed T2DM Mice

Given that HFD intake is known to induce myocardial fibrosis, we next assessed whether GLPs confer protection against fibrotic remodeling in T2DM. Masson's trichrome staining revealed that GLP treatment suppressed fibrotic re-

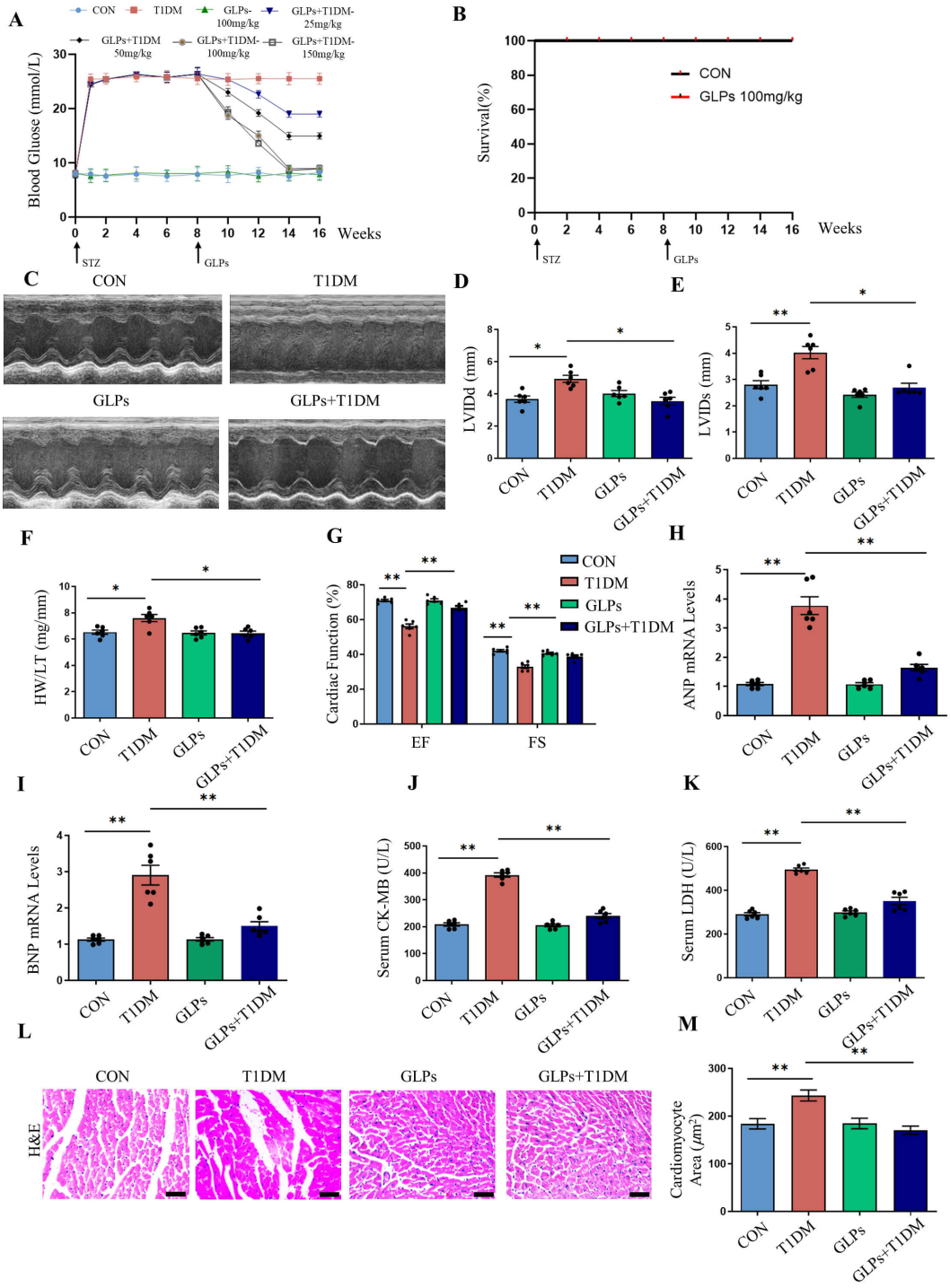


Fig. 1. *Ganoderma lucidum* polysaccharide (GLPs) treatment alleviates cardiac functional and structural impairments in streptozotocin (STZ)-induced type 1 diabetes mellitus (T1DM) mice. (A) Murine blood glucose levels. (B) Survival curve of mice treated with GLPs (100 mg/kg) and vehicle (n = 6 per group, biological duplications). (C) Representative M-mode tracings of left ventricular geometry. (D,E) Quantification of (D) LVIDd and (E) LVIDs derived from the echocardiographic data in (C) (n = 6 per group). (F) Heart weight-to-tibia length (HW/TL) ratios determined at the study endpoint (n = 6). (G) Quantitative analysis of EF% and FS% from (C) (n = 6 per group). (H,I) Relative mRNA expression of (H) *Anp* and (I) *Bnp* in cardiac tissues, as determined by RT-qPCR (n = 6 per group). (J,K) Serum concentrations of (J) creatine kinase-MB (CK-MB) and (K) lactate dehydrogenase (LDH) in each experimental group (n = 6). (L) Representative photomicrographs of hematoxylin and eosin (H&E)-stained myocardial sections (scale bars: 100 μm). (M) Quantitative assessment of cardiomyocyte cross-sectional area (n ≥ 50 cells per group). Data are mean ± standard error of the mean (SEM); *$p < 0.05$, **$p < 0.01$ vs. control mice (CON) and T1DM vs. GLPs+T1DM.

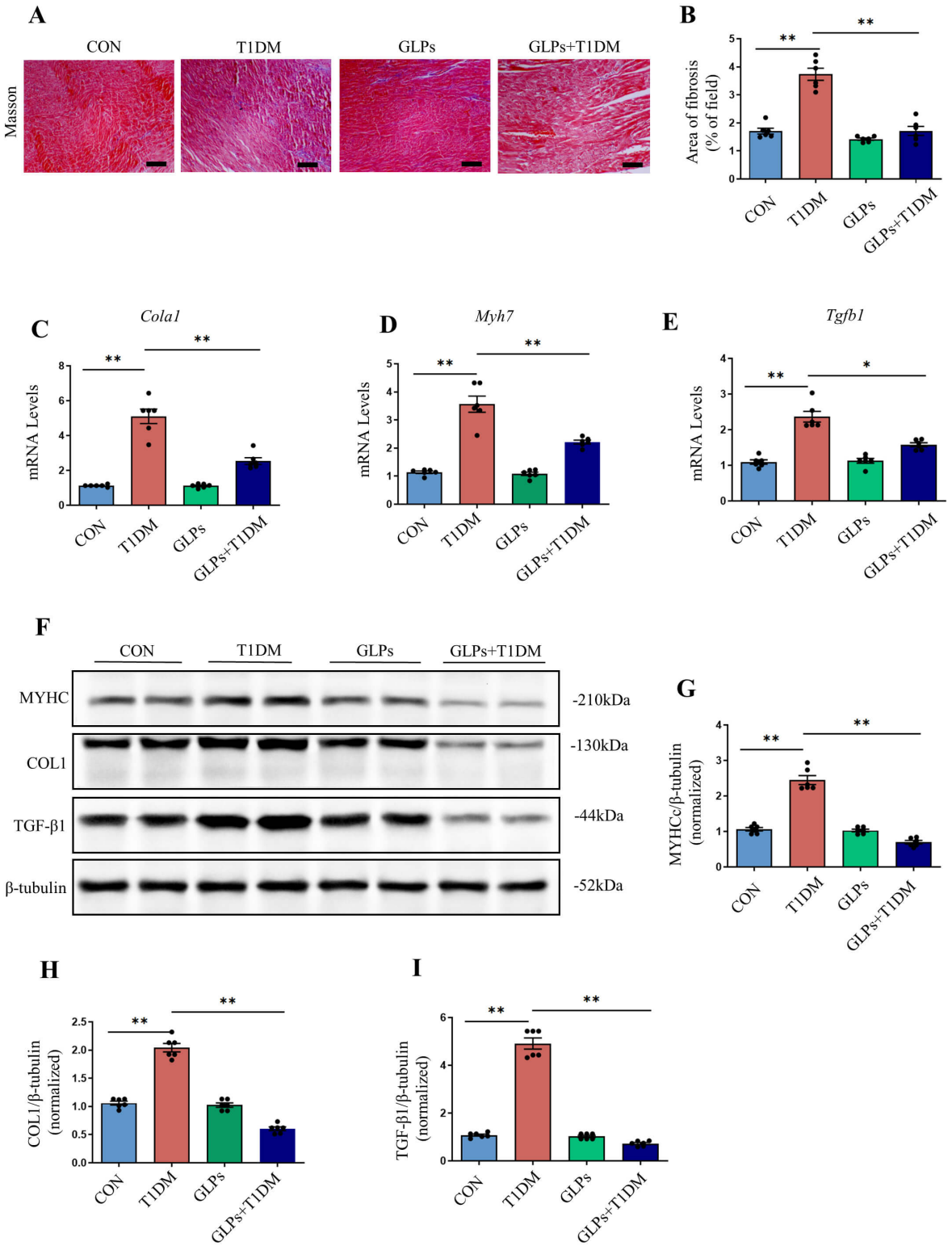


Fig. 2. GLPs attenuate STZ-induced cardiac fibrosis in mice. (A) Representative Masson's trichrome-stained myocardial sections illustrating collagen deposition (blue) (scale bars: 100 μm). (B) Quantitative analysis of interstitial fibrotic area in cardiac tissues ($n = 6$ per group). (C–E) Cardiac mRNA levels of (C) *Cola1*, (D) *Myh7*, and (E) *Tgfb1* were assessed by RT-qPCR ($n = 6$). (F) Representative Western blotting results for fibrosis-associated markers (MYHC, COL1, and TGF-β1) in myocardial lysates. (G–I) Densitometric quantification of (G) MYHC, (H) COL1, and (I) TGF-β1 protein levels corresponding to (F) ($n = 6$). Data are expressed as mean ± SEM; *$p < 0.05$, **$p < 0.01$ vs. CON and T1DM vs. GLPs+T1DM.

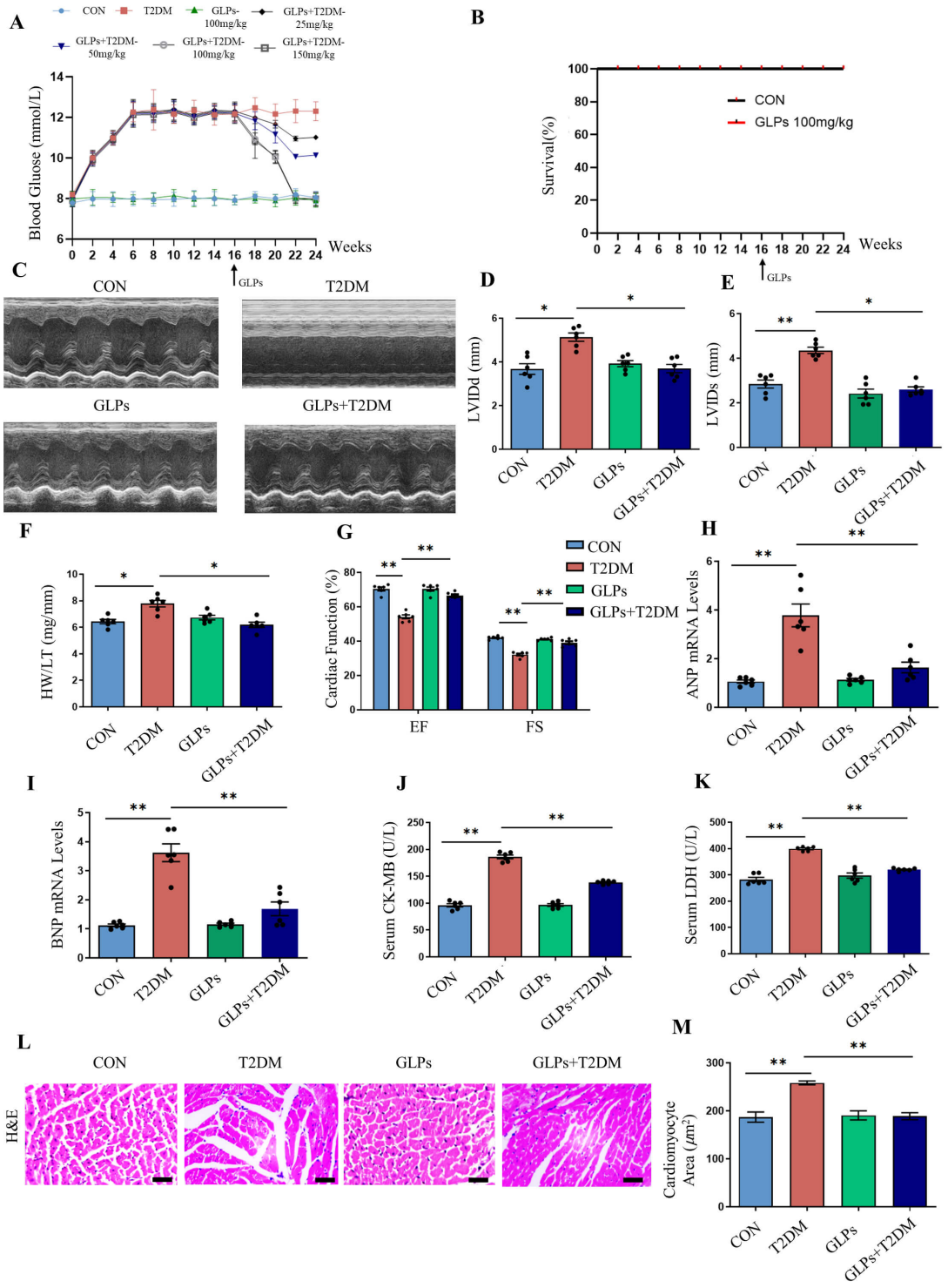


Fig. 3. GLPs mitigate HFD-induced cardiac dysfunction and structural pathology in T2DM mice. (A) Blood glucose measurements in each experimental group. (B) Survival curve of mice treated with GLPs (100 mg/kg) and vehicle ($n = 6$). (C) Representative M-mode echocardiographic tracings of the left ventricular chamber. (D,E) Quantification of (D) LVIDd and (E) LVIDs derived from (C) ($n = 6$ per group). (F) Heart weight-to-tibia length (HW/TL) ratios determined at endpoint ($n = 6$). (G) Ejection fraction (EF%) and fractional shortening (FS%) calculated from the M-mode data in (C) ($n = 6$). (H,I) Cardiac transcript levels of (H) *Anp* and (I) *Bnp* as measured by RT-qPCR ($n = 6$). (J,K) Serum concentrations of (J) CK-MB and (K) LDH ($n = 6$). (L) Representative photomicrographs of hematoxylin and eosin (H&E)-stained myocardial sections (scale bars: 100 μm). (M) Quantitative assessment of cardiomyocyte cross-sectional area ($n \geq 50$ cells per group). Data are mean ± SEM; $^{*}p < 0.05$, $^{**}p < 0.01$ vs. CON and T2DM vs. GLPs+T2DM.

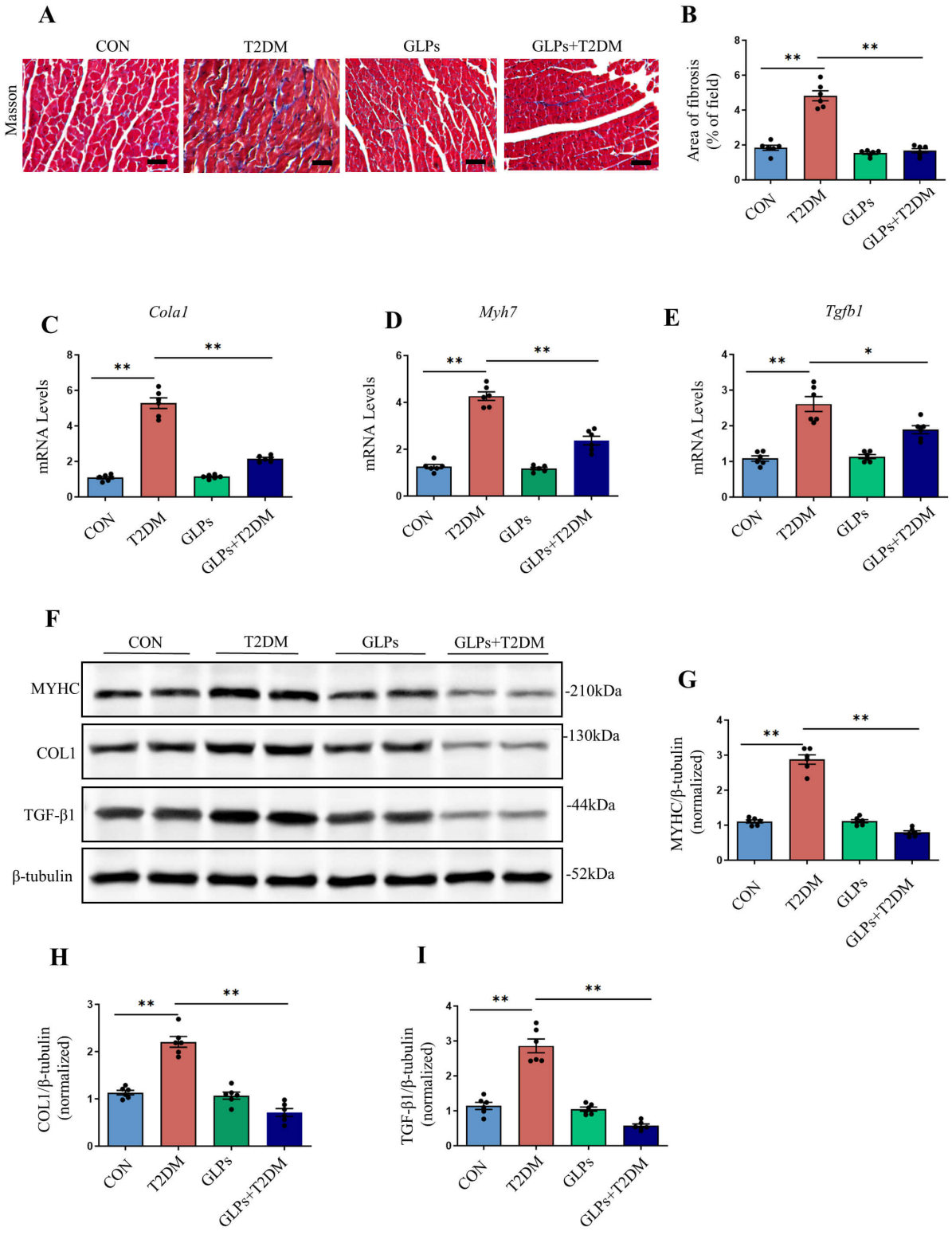


Fig. 4. GLPs ameliorate myocardial fibrosis in HFD-fed T2DM mice. (A) Representative Masson's trichrome-stained myocardial sections, with fibrotic collagen visualized in blue (scale bars: 100 μm). (B) Assessment of fibrotic changes in the myocardial interstitium (n = 6). (C–E) RT-qPCR was employed to assess the mRNA levels of *Cola1*, *Myh7*, and *Tgfb1* in myocardial samples (n = 6). (F) Representative Western blotting results for fibrotic mediators (MYHC, COL1, and TGF-β1) in myocardial lysates. (G–I) Quantification of (G) MYHC, (H) COL1, and (I) TGF-β1 from (F) (n = 6). Data are mean ± SEM; *p < 0.05, **p < 0.01 vs. CON and T2DM vs. GLPs+T2DM.

sponses, mirroring our findings in T1DM model animals (Fig. 4A,B). This was further evidenced by the downregulation of fibrotic mediators (MYHC, COL1, and TGF-β) at both transcriptional and translational levels (Fig. 4C–I). Taken together, these results confirm that GLPs mitigate cardiac fibrosis in HFD-fed T2DM mice.

3.5 GLPs Attenuate Structural Abnormalities and Remodeling in Diabetic Cardiomyopathy Through Anti-Inflammatory Activity

RNA-seq analysis of murine cardiac tissue samples revealed 840 differentially expressed genes (669 upregulated, 171 downregulated) between GLPs-treated and untreated T1DM model mice, providing a basis for exploring the cardioprotective mechanisms of GLPs against DCM (Fig. 5A). GO enrichment analysis of these differentially expressed genes revealed the significant overrepresentation of immune-inflammatory processes and NF-κB signaling, implicating these pathways in the cardioprotective effects of GLPs against DCM (Fig. 5B). A prior study found that GLPs administration in atrial fibrillation patients markedly improved cardiac outcomes, as evidenced by reductions in systolic/diastolic blood pressure, heart rate, and circulating levels of pro-inflammatory cytokines (IL-1β, IL-6, hsCRP, and TNF-α) [19]. RT-qPCR analysis confirmed the significant upregulation of *Tnf* and *Il1b* in the cardiac tissue of DCM model mice, while this induction was reversed by GLPs treatment (Fig. 5C,D). Immunohistochemical staining for the inflammatory markers CD45 and CD68 was also performed [33], revealing that GLPs reduced the number of CD45+ and CD68+ cells relative to the DCM group, indicating that GLPs attenuated the DCM-associated inflammatory infiltration in the myocardium/cardiac tissue (Fig. 5E,F).

In vitro experiments further confirmed that GLPs suppressed DCM-induced cardiomyocyte hypertrophy and inflammation. NRVMs were pretreated with 50 mg/mL GLPs for 1 hour and then exposed to HG (33 mM) conditions. This HG exposure significantly increased cardiomyocyte size, while this effect was abrogated by GLP pretreatment (Fig. 6A,B). At 12 hours post-stimulation, HG-treated NRVMs showed elevated mRNA and protein levels of fibrotic markers (MYHC, COL1, and TGF-β), whereas GLPs-pretreated cells exhibited no corresponding upregulation (Fig. 6C–E). Furthermore, GLPs pretreatment markedly suppressed the transcriptional expression of pro-inflammatory cytokines (IL-1β, TNF-α, and IL-6) under HG conditions (Fig. 6F). Collectively, these findings indicate that GLPs mitigate DCM-associated structural remodeling and fibrosis through attenuation of inflammatory responses.

3.6 Protective Effects of GLPs Involve NF-κB Signaling

GO pathway analysis identified the NF-κB cascade as one of the top three signaling pathways in the T1DM and GLP-treated T1DM groups. Given the established anti-inflammatory role of GLPs involving NF-κB Signaling, these data imply that the modulation of this NF-κB axis is central to the cardioprotective benefits of GLPs [21,22,23]. Based on the known anti-inflammatory property of GLPs through NF-κB Signaling, we hypothesized that GLPs protect against DCM via this pathway. To test this, we examined NF-κB activation *in vivo* and *in vitro*. In the hearts of T1DM model mice, enhanced IκBα and p65 phosphorylation was observed, while this increase was reversed by GLPs treatment (Fig. 7A,B), with similar findings in HFD-fed T2DM mice (Fig. 7C,D). In cultured NRVMs, HG stimulation similarly increased phosphorylated IκBα and p65 levels and promoted p65 nuclear translocation, all of which were prevented by GLPs (Fig. 7E–H). Thus, GLPs confer cardioprotection in DCM at least in part through effects on the NF-κB signaling cascade.

4. Discussion

The cardioprotective efficacy of GLPs in the context of DCM was herein evaluated using STZ-induced and obesity-associated murine models of diabetes. In both of these experimental settings, GLPs treatment consistently attenuated cardiac hypertrophy, fibrosis, dysfunction, and inflammation. Mechanistically, HG stimulation activated NF-κB signaling in diabetic hearts and HG-exposed cardiomyocytes, upregulating *Tnf*, *Il-6*, and *Il-1b* expression while promoting fibrotic and functional decline. GLP administration effectively counteracted these pathological changes, reversing cardiac remodeling. Collectively, these findings demonstrate that GLPs confer broad-spectrum cardioprotection against DCM irrespective of diabetic etiology.

DCM is defined as a diabetes-related cardiac disorder characterized by heart failure in the absence of coronary artery disease or valvular pathology [34]. Chronic low-grade inflammation plays a pivotal role in DCM development [35]. In diabetic hearts, this inflammatory state is characterized by the upregulation of adhesion molecules (ICAM-1/VCAM-1), immune cell infiltration, and elevated levels of pro-inflammatory cytokines (IL-1β, IL-6, IL-18, TNF-α) and TGF-β1 [36]. Local pro-inflammatory cytokine production can exacerbate oxidative stress, cardiac remodeling, and fibrosis, thereby contributing to the onset and progression of myocardial damage. Persistent cytokine activation is closely associated with NF-κB activation and IL-1β secretion, leading to cardiomyocyte apoptosis and necrotic death [34]. The NF-κB signaling pathway is a core transcriptional regulator of multiple inflammatory cytokines, and its activity is enhanced in the context of the inflammatory progression of DCM [37]. The anti-inflammatory effects of GLP administration in various diseases have largely been attributed to the suppression of the NF-κB pathway [22,24,38]. Consistently, GLPs treatment in the present study alleviated DCM-associated car-

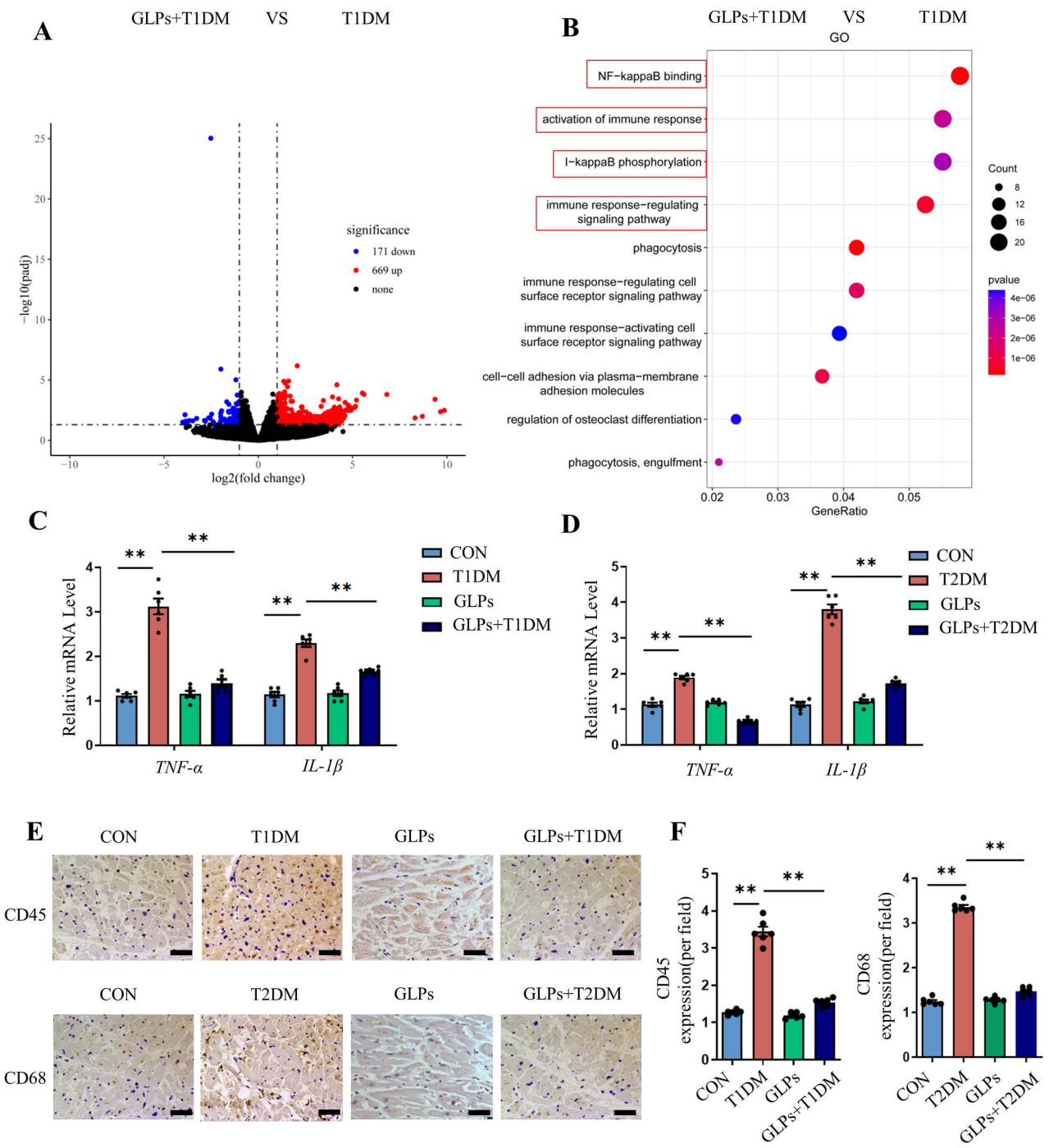


Fig. 5. GLPs alleviate diabetic cardiomyopathy by attenuating inflammatory responses. (A) Volcano plot depicting differentially expressed genes (DEGs) between the T1DM+GLPs and T1DM groups. (B) GO pathway enrichment analysis of the identified DEGs (T1DM+GLPs vs. T1DM). (C,D) RT-qPCR quantification of *Tnf-α* and *Il-1β* mRNA levels in cardiac tissue from the (C) T1DM and (D) T2DM model mice ($n = 6$ per group). (E) Representative immunostaining of cardiac sections for CD45 and CD68 (scale bars: 100 μm), with (F) corresponding quantification of positive staining areas ($n = 6$). Data are mean ± SEM; $^{**}p < 0.01$ vs. CON, T1DM vs. GLPs+T1DM and T2DM vs. GLPs+T2DM.

diac structural damage and remodeling by suppressing inflammatory responses, exerting protective effects likely associated with the NF-κB signaling pathway.

Our prior work established the ability of GLPs to inhibit cardiac hypertrophy via downregulating fibrosis-/hypertrophy-associated genes and alleviating pressure

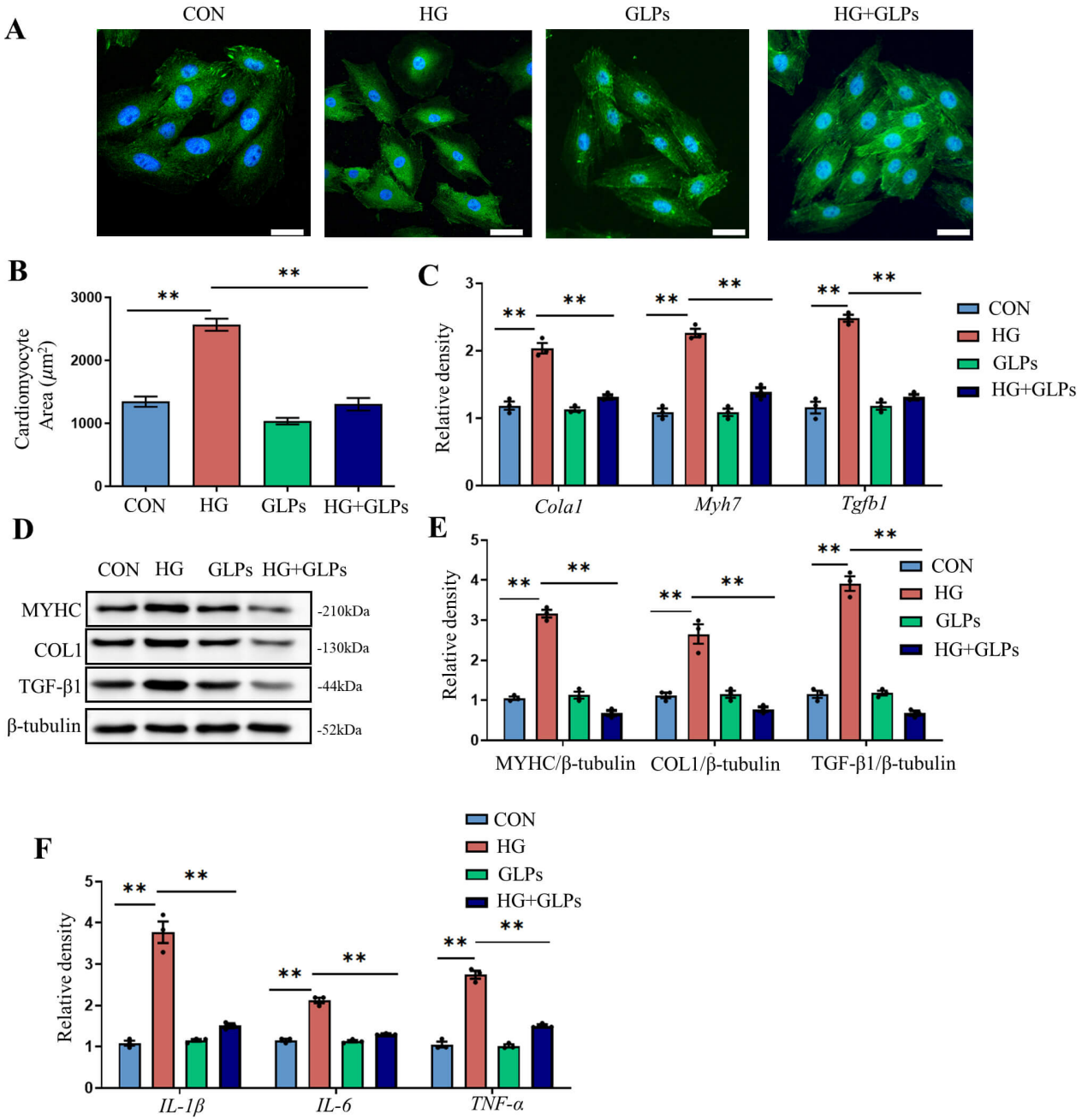


Fig. 6. GLPs mitigate high-glucose-induced hypertrophic and pro-inflammatory changes in NRVMs. (A) Immunofluorescence staining of NRVMs for α-actinin (green) and nuclei (DAPI, blue) under HG (33 mM) stimulation with or without GLP (50 mg/mL) treatment. Original magnification ×200, scale bars = 50 μm. (B) Quantification of myocyte surface area ($n \geq 50$ cells/group). (C) RT-qPCR analysis of *Cola1*, *Myh7*, and *Tgfb1* mRNA levels in NRVMs ($n = 3$). (D) Representative Western blots for fibrotic proteins (MYHC, COL1, TGF-β1) in NRVM lysates, with (E) corresponding densitometric quantification ($n = 3$). (F) RT-qPCR analysis of pro-inflammatory cytokine transcripts (*Tnf, Il-6, Il-1β*) in NRVMs ($n = 3$). Data are mean ± SEM; $^{**}p < 0.01$ vs. CON and HG vs. HG+GLPs.

overload-induced hypertrophy through PPARγ activation [20]. Since GLPs also exhibit hypoglycemic activity [39,40], in the present study we extended our investigation to DCM in an effort to determine whether GLPs exert protective effects in this diabetes-related form of cardiac pathology and to clarify the underlying mechanisms. This work not only confirms the anti-hypertrophic efficacy of this traditional Chinese medicinal extract but also expands its therapeutic potential to DCM and other cardiovascular disorders.

The therapeutic effects of GLPs on DCM are likely to be more direct and pronounced in the context of T2DM, as

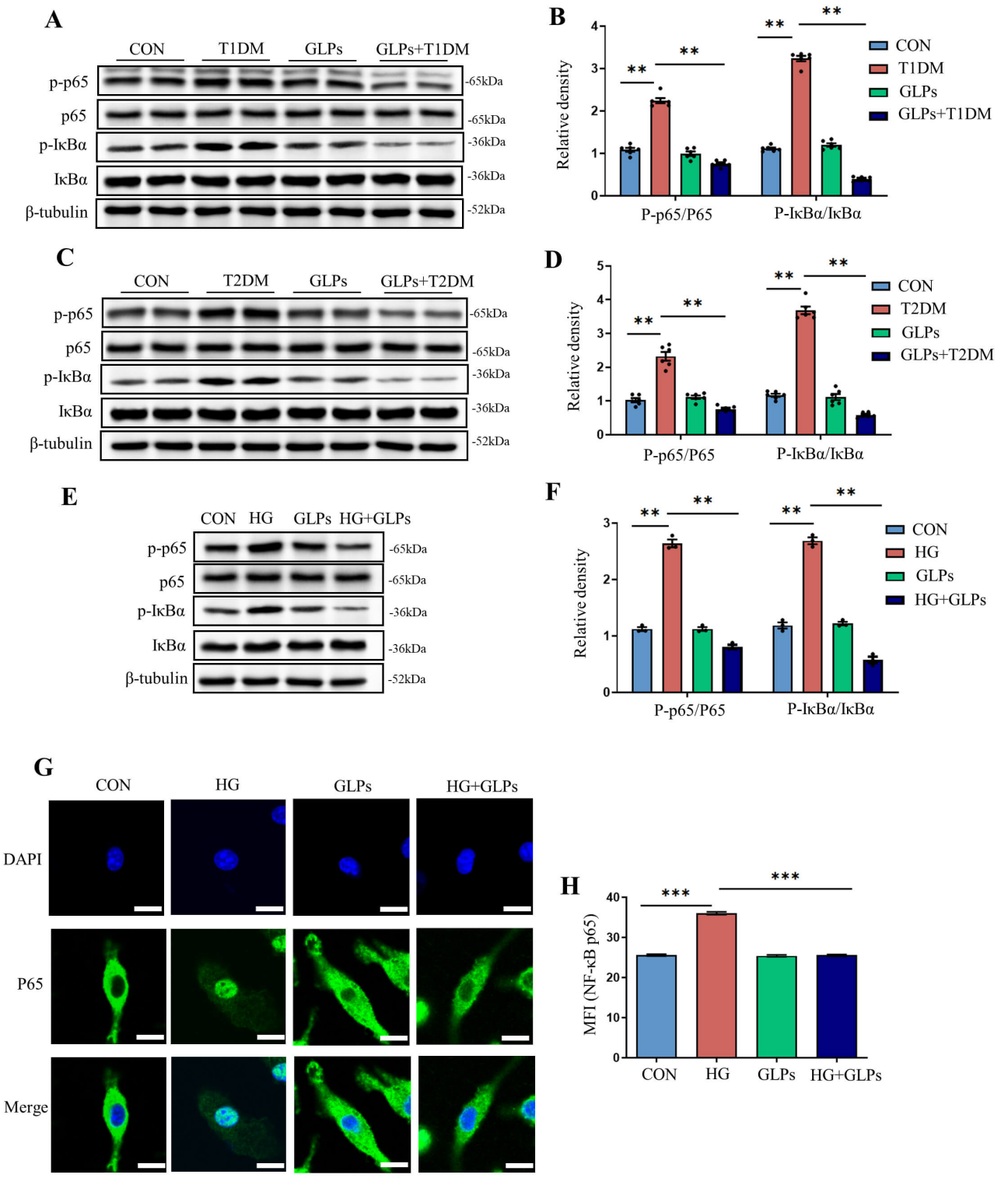


Fig. 7. Protective effects of GLPs involve NF-κB signaling. (A–D) Representative immunoblots and densitometric quantification of phosphorylated IκBα and p65 levels in cardiac lysates from (A) T1DM and (C) T2DM model mice (n = 6 per group). (E,F) Western blotting analyses of phosphorylated IκBα and p65 levels in NRVMs, with corresponding densitometric quantification (n = 3). (G) Immunofluorescence staining of NRVMs for p65 (green) with DAPI (blue) as a nuclear counterstain (scale bars: 50 μm; ×200), and (H) quantification of nuclear p65 fluorescence intensity. All data are mean ± SEM; $^{**}p < 0.01$, $^{***}p < 0.001$ vs. CON, T1DM vs. GLPs+T1DM, T2DM vs. GLPs+T2DM and HG vs. HG+GLPs.

their pharmacological targets are highly congruent with the core pathophysiological hallmarks of T2DM, namely insulin resistance and metabolic inflammation. In contrast, in T1DM, the beneficial effects of GLPs may rely more heavily on the suppression of downstream hyperglycemia-induced damage, such as oxidative stress and fibrosis, whereas their capacity to influence the fundamental etiology of the disease remains limited. Collectively, GLPs demonstrate greater potential and more well-defined mechanistic support in the treatment of T2DM-related cardiomyopathy. In T1DM, their role is instead likely auxiliary, affording cardioprotection primarily through antioxidative and anti-inflammatory effects, rather than serving as an etiology-directed therapy.

The present study has several limitations that warrant consideration. For one, the mechanistic basis for GLPs-mediated NF-κB inhibition remains incompletely understood, although TLR signaling may be involved, given that TLR activation converges on the NF-κB signaling axis [41]. The cardioprotective effects of GLPs may also be attributable to other pathways, including the PI3K-Akt axis, the dysfunction of which is linked to diabetes given its integral role in glucose metabolism [42]. Future work will be required to dissect the precise signaling cascades responsible for the protective effects of GLPs in DCM.

Hyperglycemia and glucotoxicity induce protein glycation, leading to increased formation of advanced glycation end products (AGEs). AGE deposition, in turn, promotes connective tissue cross-linking, thereby exacerbating myocardial fibrosis, increasing cardiac stiffness, and impairing diastolic relaxation [43]. Concurrently, AGEs contribute to the overproduction of reactive oxygen species (ROS), leading to enhanced inflammation and fibrotic remodeling [43]. DCM pathogenesis is also closely related to the activation of pro-inflammatory immune cells, including macrophages, dendritic cells, and activated T cells. Pro-inflammatory cytokines such as TNF-α, IL-6, and monocyte chemoattractant protein-1 (MCP-1) augment cardiac oxidative stress and coronary endothelial dysfunction, culminating in cardiac remodeling, fibrosis, and diastolic dysfunction [44]. Moreover, activation of the NF-κB signaling pathway upregulates the expression of pro-inflammatory TNF-α, IL-6, and IL-8 [44]. Both systemic and local maladaptive immune responses and inflammatory cascades thus play a pivotal role in the cardiac remodeling and fibrosis that characterizes DCM. GLPs may thus exert their cardioprotective effects both indirectly by lowering blood glucose levels to mitigate hyperglycemia-induced cardiotoxicity, and directly by suppressing the inflammatory responses that mediate cardiac injury. However, the precise mechanisms underlying these beneficial effects warrant further investigation.

Estrogen has been repeatedly demonstrated to have protective effects on the cardiovascular system while also playing an important role in maintaining normal glucose homeostasis [45,46]. Epidemiological evidence indicates that the risk of heart failure in male patients with diabetes is 2.4-fold higher than that in non-diabetic individuals, whereas in female patients this risk is increased by as much as five-fold [44]. In the present study, male mice were employed primarily to minimize the potential confounding cardioprotective and glycoregulatory effects of estrogen, thereby enabling the clearer assessment of the specific effects of GLPs on DCM. Nevertheless, the exclusion of female mice limits the generalizability of our findings. In future investigations, we will incorporate mice of both sexes to ensure that our results are more broadly applicable and to strengthen the translational relevance of our conclusions.

5. Conclusions

Collectively, our data demonstrate that GLPs exert cardioprotective effects to alleviate DCM by attenuating inflammatory responses and mitigating cardiac structural damage and that the protective effects of GLPs are involved in NF-κB signaling. These findings highlight the NF-κB pathway as a key mediator of the protective benefits of GLPs administration and provide a mechanistic rationale for their potential therapeutic application in DCM.

Abbreviations

Ang II, angiotensin II; ANP, atrial natriuretic peptide; BNP, B-type natriuretic peptide; CON, control; COL1, collagen type I; DCM, diabetic cardiomyopathy; EF, ejection fraction; FS, fractional shortening; GLPs, *Ganoderma lucidum* polysaccharides; H&E, hematoxylin and eosin; HW/TL, heart weight/ tibia length; IκBα, inhibitor of NF-κB-α; LVIDd, end-diastolic left ventricular internal dimension; LVIDs, end-systolic left ventricular internal dimension; MYHC, myosin heavy chain; NF-κB, nuclear factor-kappa B; PBS, phosphate buffered saline; RT-qPCR, reverse transcription-quantitative real-time polymerase chain reaction; STZ, streptozotocin; TAC, transverse aortic constriction; TGF-β1, transforming growth factor-β; T1DM, type 1 diabetes mellitus; T2DM, type 2 diabetes mellitus; WT, wild-type; α-SMA, α-smooth muscle actin; β-MHC, beta-myosin heavy chain.

Availability of Data and Materials

The raw sequence data reported in this paper have been deposited in the Genome Sequence Archive (Genomics, Proteomics & Bioinformatics 2025) in the National Genomics Data Center (Nucleic Acids Res 2026), China National Center for Bioinformation/Beijing Institute of Genomics, Chinese Academy of Sciences (GSA: CRA043295) that are publicly accessible at https://ngdc.cncb.ac.cn/gsa. This study did not generate any new code. All data are publicly available as of the date of publication. The other datasets used and analyzed during the current study are available from the corresponding author on reasonable request.

Author Contributions

CZ and GL conceived and designed the experiments; CZ performed the experiments; FC, DL, XH, JM and YY analyzed and interpreted the data; CZ, XH, YY and JM contributed reagents, materials, analysis tools and analyzed data; CZ wrote the paper. All authors contributed to editorial changes in the manuscript. All authors read and approved the final manuscript. All authors have participated sufficiently in the work and agreed to be accountable for all aspects of the work.

Ethics Approval and Consent to Participate

This study was carried out under the approval (No. SXYZ-A-2404-0001, April 23, 2024) of the Animal Experimentation Ethics Committee at Chongqing Three Gorges Medical College, strictly following both institutional and international animal welfare guidelines. All possible measures were taken to reduce animal discomfort, and the institutional Animal Experiment Center furnished specific training on animal husbandry and handling for all researchers involved. All animal procedures were conducted in accordance with the ARRIVE guidelines for the reporting of animal research. The study was performed in compliance with the national guidelines of China, including the Guidelines for the Care and Use of Laboratory Animals (GB/T 35892-2018).

Acknowledgment

We would like to express our gratitude to all those who helped us during the writing of this manuscript. The Graphical Abstract was drawn using Adobe Illustrator (San Jose, CA, USA).

Funding

This research was supported by the Natural Science Foundation of Chongqing, China (No. CSTB2024NSCQ-MSX0116), the Special Program for High-level Talents at Chongqing Three Gorges Medical College (No. 060203010010008) and the Science and Technology Research Program of Chongqing Municipal Education Commission (No. KJZD-K202402706, No. KJQN202302711 and No. KJQN202102701).

Conflicts of Interest

The authors declare no competing financial or personal interests that could have influenced the work reported herein. Despite FC being affiliated with Chongqing Tangshikang Medical Technology Co., Ltd., the judgments in data interpretation and writing were not influenced by this relationship.

Supplementary Material

Supplementary material associated with this article can be found, in the online version, at https://doi.org/10.31083/FBL54858.

References

[1] Marín-García J, Akhmedov AT. Mitochondrial dynamics and cell death in heart failure. Heart Failure Reviews. 2016; 21: 123–136. https://doi.org/10.1007/s10741-016-9530-2

[2] Han X, Zheng R, Zhang J, Liu Y, Li Z, Liu G, et al. Cardiomyocyte OTUD1 drives diabetic cardiomyopathy via directly deubiquitinating AMPKα2 and inducing mitochondrial dysfunction. Nature Communications. 2025; 16: 6668. https://doi.org/10.1038/s41467-025-61901-z

[3] Niu W, Liu X, Deng B, Hong T, Wang C, Yan Y, et al. Piezo1 deletion mitigates diabetic cardiomyopathy by maintaining mitochondrial dynamics via ERK/Drp1 pathway. Cardiovascular Diabetology. 2025; 24: 127. https://doi.org/10.1186/s12933-025-02625-8

[4] Han X, Huang Z, Liu G, Liu Y, Li W, Zheng J, et al. VCPIP1 drives diabetic cardiomyopathy by deubiquitinating AMPKγ1 and preventing AMPKα-γ subunit assembly in cardiomyocytes. Signal Transduction and Targeted Therapy. 2026; 11: 185. https://doi.org/10.1038/s41392-026-02701-9

[5] McLean E, Roo C, Maag A, Coble M, Cano J, Liu R. ERK1/2 Inhibition Alleviates Diabetic Cardiomyopathy by Suppressing Fatty Acid Metabolism. Frontiers in Bioscience (Landmark Edition). 2025; 30: 26700. https://doi.org/10.31083/FBL26700

[6] Zheng H, Zhu H, Liu X, Huang X, Huang A, Huang Y. Mitophagy in Diabetic Cardiomyopathy: Roles and Mechanisms. Frontiers in Cell and Developmental Biology. 2021; 9: 750382. https://doi.org/10.3389/fcell.2021.750382

[7] Murtaza G, Virk HUH, Khalid M, Lavie CJ, Ventura H, Mukherjee D, et al. Diabetic cardiomyopathy - A comprehensive updated review. Progress in Cardiovascular Diseases. 2019; 62: 315–326. https://doi.org/10.1016/j.pcad.2019.03.003

[8] Ramesh P, Yeo JL, Brady EM, McCann GP. Role of inflammation in diabetic cardiomyopathy. Therapeutic Advances in Endocrinology and Metabolism. 2022; 13: 20420188221083530. https://doi.org/10.1177/20420188221083530

[9] Frati G, Schirone L, Chimenti I, Yee D, Biondi-Zoccai G, Volpe M, et al. An overview of the inflammatory signalling mechanisms in the myocardium underlying the development of diabetic cardiomyopathy. Cardiovascular Research. 2017; 113: 378–388. https://doi.org/10.1093/cvr/cvx011

[10] Jiang MY, Zhang XH, Zhang HL, Hou Y, Qi MY, Zuo YX, et al. GULP1 protects against diabetic cardiomyopathy through IKIP/NF-κB-dependent improvement of mitochondrial function. Cardiovascular Diabetology. 2026; 25: 170. https://doi.org/10.1186/s12933-026-03184-2

[11] Hassan N, Mohamed M, Hassan NA, Mohammed HO, Abdelmoniem HO, Al-Zayat KA, et al. Delonix regia flower extract protects against diabetic cardiac remodeling via modulating eNOS/NO/cGMP and NF-κB/iNOS/TNF-α trajectories. The Journal of Pharmacy and Pharmacology. 2026; 78: rgag024. https://doi.org/10.1093/jpp/rgag024

[12] Zhou X, Xing S, Zhang L, Lu J, Li D, Wang Y, et al. Amniotic mesenchymal stem cells attenuate diabetic cardiomyopathy by inhibiting pyroptosis via modulation of the TLR4/NF-κb/NLRP3 pathway. Frontiers in Cell and Developmental Biology. 2025; 13: 1631973. https://doi.org/10.3389/fcell.2025.1631973

[13] Sharma P, Tulsawani R, Agrawal U. Pharmacological effects of Ganoderma lucidum extract against high-altitude stressors and its subchronic toxicity assessment. Journal of Food Biochemistry. 2019; 43: e13081. https://doi.org/10.1111/jfbc.13081

[14] Ahmad MF, Ahmad FA, Hasan N, Alsayegh AA, Hakami O, Bantun F, et al. Ganoderma lucidum: Multifaceted mechanisms to combat diabetes through polysaccharides and triterpenoids: A comprehensive review. International Journal of Biological

Macromolecules. 2024; 268: 131644. https://doi.org/10.1016/j.ijbiomac.2024.131644
[15] Hu Y, Wang SX, Wu FY, Wu KJ, Shi RP, Qin LH, et al. Effects and Mechanism of Ganoderma lucidum Polysaccharides in the Treatment of Diabetic Nephropathy in Streptozotocin-Induced Diabetic Rats. BioMed Research International. 2022; 2022: 4314415. https://doi.org/10.1155/2022/4314415
[16] Zheng J, Yang B, Yu Y, Chen Q, Huang T, Li D. Ganoderma lucidum polysaccharides exert anti-hyperglycemic effect on streptozotocin-induced diabetic rats through affecting β-cells. Combinatorial Chemistry & High Throughput Screening. 2012; 15: 542–550. https://doi.org/10.2174/138620712801619168
[17] Wang Y, Zuo Y, Weng J, Peng X. Health benefits of Ganoderma lucidum polysaccharides: A review of potential cardiovascular protective effects. International Journal of Biological Macromolecules. 2025; 330: 148001. https://doi.org/10.1016/j.ijbiomac.2025.148001
[18] Xue H, Qiao J, Meng G, Wu F, Luo J, Chen H, et al. Effect of Ganoderma lucidum polysaccharides on hemodynamic and antioxidation in T2DM rats. Zhongguo Zhong Yao Za Zhi = Zhongguo Zhongyao Zazhi = China Journal of Chinese Materia Medica. 2010; 35: 339–343. https://doi.org/10.4268/cjcmm20100318
[19] Rizal A, Sandra F, Fadlan MR, Sargowo D. Ganoderma lucidum Polysaccharide Peptide Reduce Inflammation and Oxidative Stress in Patient with Atrial Fibrillation. The Indonesian Biomedical Journal. 2020; 12: 384–389. http://doi.org/10.18585/inabj.v12i4.1244
[20] Zhen C, Wu X, Zhang J, Liu D, Li G, Yan Y, et al. *Ganoderma lucidum* polysaccharides attenuates pressure-overload-induced pathological cardiac hypertrophy. Frontiers in Pharmacology. 2023; 14: 1127123. https://doi.org/10.3389/fphar.2023.1127123
[21] Meng M, Wang L, Yao Y, Lin D, Wang C, Yao J, et al. Ganoderma lucidum polysaccharide peptide (GLPP) attenuates rheumatic arthritis in rats through inactivating NF-κB and MAPK signaling pathways. Phytomedicine: International Journal of Phytotherapy and Phytopharmacology. 2023; 119: 155010. https://doi.org/10.1016/j.phymed.2023.155010
[22] Jiang Y, Wang Z, Wang W, Liu Y, Meng Y, Wang Y, et al. Ganoderma lucidum polysaccharide alleviates cognitive dysfunction by inhibiting neuroinflammation via NLRP3/NF-κB signaling pathway. Journal of Ethnopharmacology. 2025; 338: 119065. https://doi.org/10.1016/j.jep.2024.119065
[23] Shi D, Xu X, Wang J, Bu T, Sun P, Yang K, et al. Synergistic anti-inflammatory effects of Ganoderma lucidum polysaccharide and ganoderic acid A on LPS-induced RAW264.7 cells by inhibition of TLR4/NF-κB activation. International Journal of Biological Macromolecules. 2025; 309: 143074. https://doi.org/10.1016/j.ijbiomac.2025.143074
[24] Zhao H, Li Y, Liu N, Chen P, Yu X, Li G, et al. Ganoderma lucidum polysaccharides alleviate non-alcoholic fatty liver disease by modulating gut microbiota against TLR4/NF-κB/MAPK pathway and activating AMPK pathway. Journal of Ethnopharmacology. 2026; 355: 120723. https://doi.org/10.1016/j.jep.2025.120723
[25] Wang M, Jin L, Zhang Q, Zhu W, He H, Lou S, et al. Curcumin analog JM-2 alleviates diabetic cardiomyopathy inflammation and remodeling by inhibiting the NF-κB pathway. Biomedicine & Pharmacotherapy. 2022; 154: 113590. https://doi.org/10.1016/j.biopha.2022.113590
[26] Heydemann A. An Overview of Murine High Fat Diet as a Model for Type 2 Diabetes Mellitus. Journal of Diabetes Research. 2016; 2016: 2902351. https://doi.org/10.1155/2016/2902351
[27] Hasan P, Saotome M, Ikoma T, Iguchi K, Kawasaki H, Iwashita T, et al. Mitochondrial fission protein, dynamin-related protein 1, contributes to the promotion of hypertensive cardiac hypertrophy and fibrosis in Dahl-salt sensitive rats. Journal of Molecular and Cellular Cardiology. 2018; 121: 103–106. https://doi.org/10.1016/j.yjmcc.2018.07.004
[28] He C, Medley SC, Hu T, Hinsdale ME, Lupu F, Virmani R, et al. PDGFRβ signalling regulates local inflammation and synergizes with hypercholesterolaemia to promote atherosclerosis. Nature Communications. 2015; 6: 7770. https://doi.org/10.1038/ncomms8770
[29] Zhou C, Kuang M, Tao Y, Wang J, Luo Y, Fu Y, et al. Nynrin preserves hematopoietic stem cell function by inhibiting the mitochondrial permeability transition pore opening. Cell Stem Cell. 2024; 31: 1359–1375.e8. https://doi.org/10.1016/j.stem.2024.06.007
[30] Picelli S, Faridani OR, Björklund AK, Winberg G, Sagasser S, Sandberg R. Full-length RNA-seq from single cells using Smart-seq2. Nature Protocols. 2014; 9: 171–181. https://doi.org/10.1038/nprot.2014.006
[31] Kuwahara K. The natriuretic peptide system in heart failure: Diagnostic and therapeutic implications. Pharmacology & Therapeutics. 2021; 227: 107863. https://doi.org/10.1016/j.pharmthera.2021.107863
[32] Gaggin HK, Januzzi JL, Jr. Biomarkers and diagnostics in heart failure. Biochimica et Biophysica Acta. 2013; 1832: 2442–2450. https://doi.org/10.1016/j.bbadis.2012.12.014
[33] Li D, Guo YY, Cen XF, Qiu HL, Chen S, Zeng XF, et al. Lupeol protects against cardiac hypertrophy via TLR4-PI3K-Akt-NF-κB pathways. Acta Pharmacologica Sinica. 2022; 43: 1989–2002. https://doi.org/10.1038/s41401-021-00820-3
[34] Jia G, Hill MA, Sowers JR. Diabetic Cardiomyopathy: An Update of Mechanisms Contributing to This Clinical Entity. Circulation Research. 2018; 122: 624–638. https://doi.org/10.1161/CIRCRESAHA.117.311586
[35] Bellemare M, Bourcier L, Iglesies-Grau J, Boulet J, O'Meara E, Bouabdallaoui N. Mechanisms of diabetic cardiomyopathy: Focus on inflammation. Diabetes, Obesity & Metabolism. 2025; 27: 2326–2338. https://doi.org/10.1111/dom.16242
[36] Battiprolu PK, Lopez-Crisosto C, Wang ZV, Nemchenko A, Lavandero S, Hill JA. Diabetic cardiomyopathy and metabolic remodeling of the heart. Life Sciences. 2013; 92: 609–615. https://doi.org/10.1016/j.lfs.2012.10.011
[37] Zou F, Wang L, Liu H, Wang W, Hu L, Xiong X, et al. Sophocarpine Suppresses NF-κB-Mediated Inflammation Both *In Vitro* and *In Vivo* and Inhibits Diabetic Cardiomyopathy. Frontiers in Pharmacology. 2019; 10: 1219. https://doi.org/10.3389/fphar.2019.01219
[38] Yang T, Fang H, Lin D, Yang S, Luo H, Wang L, et al. Ganoderma Lucidum polysaccharide peptide (GL-PP2): A potential therapeutic agent against sepsis-induced organ injury by modulating Nrf2/NF-κB pathways. International Journal of Biological Macromolecules. 2025; 285: 138378. https://doi.org/10.1016/j.ijbiomac.2024.138378
[39] Xiao C, Wu Q, Xie Y, Tan J, Ding Y, Bai L. Hypoglycemic mechanisms of Ganoderma lucidum polysaccharides F31 in db/db mice via RNA-seq and iTRAQ. Food & Function. 2018; 9: 6495–6507. https://doi.org/10.1039/c8fo01656a
[40] Li F, Zhang Y, Zhong Z. Antihyperglycemic effect of ganoderma lucidum polysaccharides on streptozotocin-induced diabetic mice. International Journal of Molecular Sciences. 2011; 12: 6135–6145. https://doi.org/10.3390/ijms12096135
[41] Chen J, Zhang L, Shu Y, Chen L, Zhu M, Yao S, et al. Curcumin Analogue CA15 Exhibits Anticancer Effects on HEp-2 Cells via Targeting NF-κB. BioMed Research International. 2017; 2017: 4751260. https://doi.org/10.1155/2017/4751260
[42] Huang X, Liu G, Guo J, Su Z. The PI3K/AKT pathway in obesity

and type 2 diabetes. International Journal of Biological Sciences. 2018; 14: 1483–1496. https://doi.org/10.7150/ijbs.27173

[43] Jia G, DeMarco VG, Sowers JR. Insulin resistance and hyperinsulinaemia in diabetic cardiomyopathy. Nature Reviews. Endocrinology. 2016; 12: 144–153. https://doi.org/10.1038/nrendo.2015.216

[44] Jia G, Whaley-Connell A, Sowers JR. Diabetic cardiomyopathy: a hyperglycaemia- and insulin-resistance-induced heart disease. Diabetologia. 2018; 61: 21–28. https://doi.org/10.1007/s00125-017-4390-4

[45] Paquin A, Iribarren AC. Editorial Commentary to Unveiling Estrogen's Protective Power in Women's Cardiovascular Health. The Canadian Journal of Cardiology. 2025; 41: 1428–1429. https://doi.org/10.1016/j.cjca.2025.03.020

[46] Shan W, Ding J, Xu J, Du Q, Chen C, Liao Q, et al. Estrogen regulates duodenal glucose absorption by affecting estrogen receptor-α on glucose transporters. Molecular and Cellular Endocrinology. 2023; 112028. https://doi.org/10.1016/j.mce.2023.112028